(25) M. Yoshifuji, M. Loots, and J. Schwartz, *Tetrahedron Lett.*, 1303 (1977).
(26) B. Kautzner, P. C. Wailes, and H. Weigold, *Chem. Commun.*, 1105 (1965).
(27) D. W. K. Yeung and J. Warkentin, *Can. J. Chem.*, **54**, 1345 (1976).
(28) (a) C. J. Pouchert, Ed., "The Aldrich Library of Infrared Spectra", Vol. 2, Aldrich Chemical Co., Milwaukee, Wis., 1975, p 748B; (b) C. J. Pouchert and J. R. Campbell, Eds., "The Aldrich Library of NMR Spectra", Vol. 6, Aldrich Chemical Co., Milwaukee, Wis., 1974, p 9C.
(29) R. Barlet, M. Montagne, and P. Arnaud, *Spectrochim. Acta*, **25**, 1081 (1969).
(30) P. W. Hickmott, B. J. Hopkins, and C. T. Yoxall, *J. Chem. Soc. B*, 205 (1971).
(31) Y. Bahurel, F. Collonges, A. Menet, F. Pautet, A. Poncet, and G. Descotes, *Bull. Soc. Chim. Fr.*, 2209 (1971).
(32) "Sadtler Standard Spectra", Sadtler Research Laboratories, Philadelphia, Pa., No. IR 16657.
(33) See ref 28, No. IR 88C, NMR 108C.
(34) J. K. Crandall, J. P. Arrington, and J. Hen, *J. Am. Chem. Soc.*, **89**, 6208 (1967).
(35) See ref 28, No. IR 19103, NMR 2152M.
(36) E. Lee-Ruff, N. J. Turro, P. Amice, and J. M. Conia, *Can. J. Chem.*, **47**, 2797 (1969).
(37) G. Zweifel and G. M. Clark, *J. Organomet. Chem.*, **39**, C33 (1972).
(38) (a) A. E. Bey and D. R. Weyenberg, *J. Org. Chem.*, **30**, 2436 (1965); (b) M. Fischer and C. Djerassi, *Chem. Ber.*, **99**, 750 (1966).
(39) R. R. Arndt and C. Djerassi, *Chem. Commun.*, **22**, 578 (1965).
(40) R. Quelet, P. Bercot, and J. d'Angelo, *Bull. Soc. Chim. Fr.*, 3258 (1966).
(41) M. Neuenshwander, R. Kyberg, and R. Iseli, *Chimia*, **24**, 342 (1970).
(42) See ref 28, No. IR 499 D, NMR *4* 1D.
(43) (a) M. Stoll, M. Winter, F. Gautschi, I. Flament, and B. Willhalm, *Helv. Chim. Acta*, **50**, 628 (1967); (b) ref 28, No. IR 225 D, NMR *2* 120C.
(44) For example, the Cp position in the reaction between $Cp_2Zr(Cl)$(3,3-dimethylbutyl) and a 40% excess of $AlCl_3$ appears approximately 40% of the way between the positions of free Cp_2ZrCl_2 and the complex $Cp_2ZrCl_2 \cdot AlCl_3$. This complex is weak; it is readily destroyed (as evidenced by NMR) by weak Lewis bases such as ethers, acyl chlorides, or ketones.
(45) When transmetalation was performed between 0 and 25 °C, a small amount of isobutylene was generated as a side product; when the reaction was performed at −40 °C, no isobutylene was produced.

Resonance Raman Spectra, Excitation Profiles and Excited (Iron → Pyridine Charge Transfer) State Geometry of Bispyridine Iron(II) Heme

P. G. Wright, P. Stein, J. M. Burke, and T. G. Spiro*

Contribution from the Department of Chemistry, Princeton University, Princeton, New Jersey 08540. *Received July 3, 1978*

Abstract: Totally symmetric bound pyridine vibrational modes are observed in the resonance Raman spectra of $(py)_2Fe^{II}MP$ (py = pyridine, MP = mesoporphyrin IX dimethyl ester) and the pyridine-d_5 analogue. The frequencies and their deuterium shifts are satisfactorily calculated using a benzene force field and an Fe–N stretching force constant of 1.96 mdyn Å^{-1}. The Fe–py stretching mode is at 179 cm^{-1}. Excitation profiles show all py modes maximizing at 496.5 nm, close to a bump in the absorption spectrum at 490 nm. Approximate origin shifts are obtained from the relative Raman intensities of the py modes and are combined with the calculated eigenvectors to provide a qualitative picture of the geometry in the resonant excited state, which is assigned to $d_{\pi(Fe)} \rightarrow \pi^*_{(py)}$ charge transfer.

Introduction

Recently we reported[1] resonance-enhanced Raman scattering by bound pyridine, as well as porphyrin, modes (RR modes) of $(py)_2Fe^{II}MP$ and $(4\text{-Mepy})_2Fe^{II}MP$ (py = pyridine, 4-Mepy = 4-methylpyridine, MP = mesoporphyrin IX dimethyl ester). The pyridine modes appeared to be resonant with a bump in the absorption spectrum at ~490 nm, which might plausibly be an $Fe^{II} \rightarrow$ py charge transfer (CT) transition. This assignment had been suggested[2] for a shoulder in the $(py)_2Fe^{II}TPP$ (TPP = tetraphenylporphine) absorption spectrum at 476 nm, and RR modes of bound pyridine have also been observed for this complex.[3]

While metalloporphyrin RR spectra are dominated by in-plane vibrational modes of the porphyrin ring,[4] low-frequency modes assignable to iron–axial ligand vibrations have been observed for oxyhemoglobin[5] and a "picket fence" porphyrin analogue[3] for iron(III) octaethylporphine halides[6,7] and for methemoglobin complexes.[8] The bispyridine Fe^{II} hemes, however, appear to be the only reported instance where bound ligand modes are enhanced. It seemed of interest to characterize the process in greater detail. We present here results of a normal coordinate and intensity analysis of the bound pyridine modes in $(py)_2Fe^{II}MP$ and in its py-d_5 analogue, which give a satisfying account of the eigenvectors and of the likely geometry of the CT excited state.

Experimental Section

Mesoporphyrin IX dimethyl ester was purchased from Sigma Chemical Co. and used without further purification. Pyridine-h_5 was distilled and stored over KOH. Pyridine-d_5 was purchased from Merck Sharp and Dohme and used without further purification. Dichloromethane was distilled and stored over molecular sieve.

The preparation of $(F^-)Fe^{III}MP$ has been described previously.[1] The preparation of $(py)_2Fe^{II}MP$ was carried out in a modified Spex spinning cell sealed with a Teflon stopper. A solution of $(F^-)Fe^{III}MP$ and excess pyridine in dichloromethane was covered with a water layer. After nitrogen gas had been bubbled through the solution for ~5 min, a small amount of sodium dithionite was added. The cell was quickly sealed and vigorously shaken until the dichloromethane layer changed from red-brown to orange. The concentration of $(py)_2Fe^{II}MP$ in dichloromethane was ~1 mg/mL.

Spectra were excited with various lines of an Ar^+ laser, and recorded with a Spex 1401 double monochromator equipped with a cooled ITT FW 130 photomultiplier and photon counting electronics. Frequencies were internally calibrated against the solvent bands and are believed to be accurate to ±1 cm^{-1} for the strong bands.

Results and Discussion

Figure 1 shows RR spectra of $(py)_2Fe^{II}MP$ and $(py\text{-}d_5)_2Fe^{II}MP$ excited at 476.5 nm. The bound pyridine bands, labeled in Figure 1, are readily identified by the deuteration shifts as well as from the excitation profiles (vide infra). All of these bands are polarized and therefore arise from totally symmetric vibrations. Their frequencies are listed in Table I.

Normal Coordinate Analysis. A normal coordinate analysis, using available computer programs,[9] was carried out on a linear py–Fe–py model to obtain a qualitative picture of the

0002-7863/79/1501-3531$01.00/0

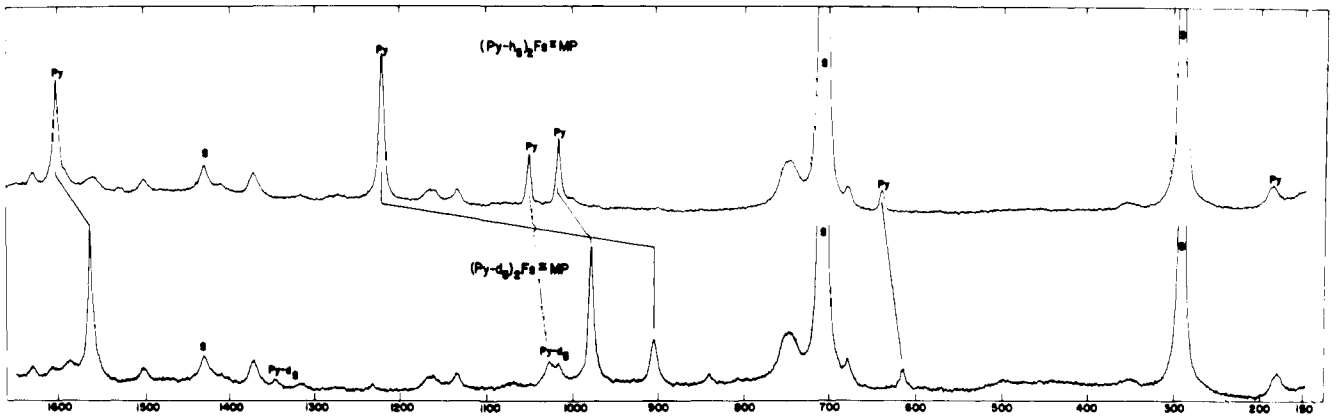

Figure 1. Resonance Raman spectra of (py-h_5)$_2$Fe^{II}MP and (py-d_5)$_2$Fe^{II}MP in CH_2Cl_2, obtained with 476.5-nm Ar^+ excitation. Bands marked "py" are assigned to the bound pyridine, those marked "S" are due to the solvent, and the remaining bands are porphyrin modes. Conditions: laser power, 220 mW; spectral slit width, 5 cm^{-1}; scan rate, 0.2 cm^{-1}/s.

Table I. Vibrational Frequencies (cm^{-1}) and Intensities of Bound Pyridine in (py)$_2$Fe^{II}MP

mode	pyridine[a]	(py-h_5)$_2$Fe^{II}MP obsd	calcd	I_{obsd}[b]	pyridine-d_5[a]	(py-d_5)$_2$Fe^{II}MP obsd	calcd	I_{obsd}[b]	I_{calcd}[d]
1	1580	1597	1620	1.0	1530	1557	1602	1.0	1.0
2	1482	[c]	1485	0.0	1340	1340	1328	0.01	0.15
3	1218	1216	1194	1.57	887	899	856	0.30	0.45
4	1068	[c]	1034	0.0	823	835	832	0.05	0.08
5	1029	1044	1077	0.31	1006	1021	1029	0.10	0.10
6	992	1010	991	0.87	962	972	945	1.0	0.72
7	605	635	653	0.07	582	609	628	0.05	0.07
8		179	179	0.07		174	173	0.05	0.05

[a] Taken from ref 13. Observed frequencies. [b] Ratioed to the 1597- and 1557-cm^{-1} bands in (py)$_2$Fe^{II}MP and (py-d_5)$_2$Fe^{II}MP, respectively. I_{obsd} = relative experimental intensity, with 496-nm excitation. [c] Not observed. [d] Calculated intensities from solution 1 of Table II.

form of the normal vibrations and to ensure that the isotopic shift observed for the lowest frequency band was consistent with its assignment to the symmetric Fe–py stretching vibration. An eclipsed conformation, giving D_{2h} molecular symmetry, was assumed. The actual rotamer population is of no significance to the calculation owing to the constraints placed on the force field. Neglect of the porphyrin is a reasonable approximation, since kinematic coupling is zero, by virtue of the orthogonality of the Fe–pyridine and Fe–pyrrole bonds. Whatever potential couplings may be operative are incorporated into the force constants of the model system. Its 43 in-plane vibrations were defined by 49 internal coordinates of the type used by Duinker and Mills for benzene.[10] The molecular parameters of free pyridine[11] were used, together with 2.05-Å Fe–N bonds.[12]

A Fe–N stretching force constant of 1.96 mdyn/Å was used. Since Fe–N bending modes are non-totally-symmetric, the associated force constants were held at very low values to effectively remove them from the calculation. Interaction force constants between the pyridine ring and the Fe–N bond and across the Fe atom were set equal to zero. The benzene force field[10] was applied directly to the pyridine coordinates. Some systematic variations were then examined. The C–N force constant was assigned a value 20% higher than the C–C force constant in view of the 0.05 Å shorter bond length. Values of the internal ring angle bend and hydrogen deformation force constants were also varied by ±5%. The qualitative features of the vibrational eigenvectors were found to be insensitive to these changes, so Duinker and Mills' benzene force field was retained for the purpose of the present analysis.

The calculated and observed frequencies are compared in Table I and the eigenvectors are shown in Figures 2a and 2b. The frequencies are reasonably well calculated, and the deuterium isotope shifts are satisfactorily reproduced. The assignments of the bound pyridine modes are parallel to those of free pyridine.[13,14] The 179-cm^{-1} band, which does not appear in free pyridine, is assigned to the symmetric py–Fe–py stretching mode, and the observed 5-cm^{-1} shift on deuteration is correctly calculated. This low value for an iron–ligand stretching mode reflects the fact that the pyridine molecules move essentially as a rigid body. An L–Fe–L triatomic model in which L is given a point mass of the molecular weight of pyridine gives nearly the correct frequency (205 cm^{-1}). The deuteration shift is also reproduced with this model and the 162-cm^{-1} band observed[1] in the RR spectrum of (4-Mepy)$_2$-Fe^{II}MP is similarly reproduced using the same force constant and the molecular weight of 4-Mepy.

Excitation Profiles. Figure 3 shows excitation profiles for well-resolved bound pyridine RR modes in (py)$_2$Fe^{II}MP, obtained with Ar^+ lines from 457.9 to 514.5 nm. Also shown is the visible absorption spectrum. The lowest energy absorption peak is the $\alpha(Q_0)$ band at 546 nm. The vibronic $\beta(Q_v)$ sideband appears to be split into two components, at 516 and 508 nm, 1065 and 1370 cm^{-1} above the α band. At still higher energy, 490 nm, is another bump which is too far (2093 cm^{-1}) from the α band to be part of the vibronic envelope.

The bound pyridine modes all come into resonance close to the 490-nm absorption band, which we therefore assign to a $Fe^{II} \rightarrow$ py charge transfer transition. All of the depolarization ratios are within experimental error of 1/3, as expected for resonance with out-of-plane transitions. The direction of the charge transfer is dictated by the availability of relatively low-lying empty π^* orbitals on pyridine and full π orbitals (d_{xz}, d_{yz}) on iron. The latter also mix with porphyrin π^* orbitals and to that extent porphyrin would also be involved in the transition. Actually several porphyrin vibrational modes show en-

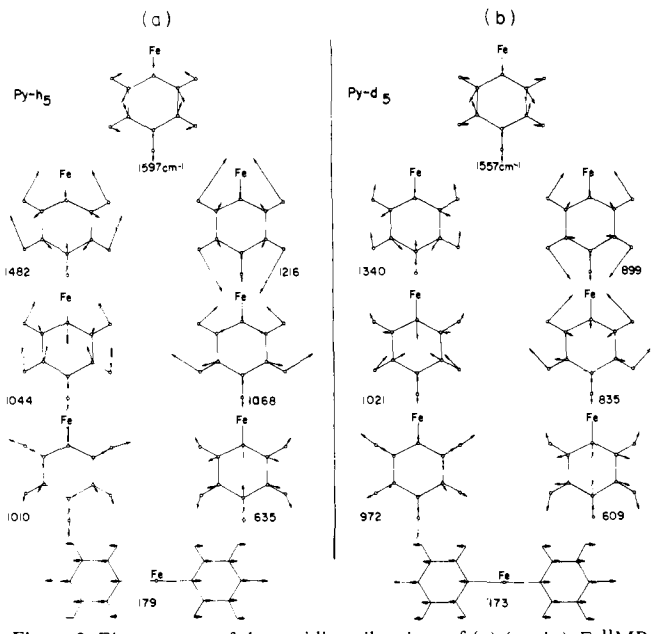

Figure 2. Eigenvectors of the pyridine vibrations of (a) (py-h_5)$_2$Fe^{II}MP and (b) (py-d_5)$_2$Fe^{II}MP. The 1482- and 1068-cm^{-1} modes are unobserved in the py-h_5 complex; the frequencies are those of free pyridine. Half the py-Fe-py unit is shown, except for the 179- (173-) cm^{-1} mode, which illustrates the mainly Fe-py stretching normal coordinate. The normal mode calculation gives negative phasing for the eigenvectors of the py-h_5 modes at 1482, 1068, 1044, and 635 cm^{-1} (and the corresponding py-d_5 modes) relative to the other four modes.

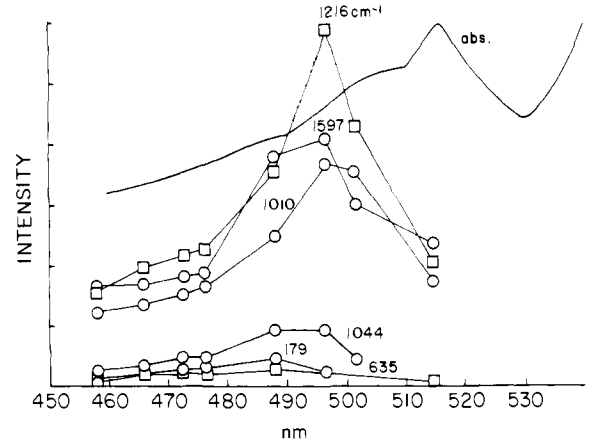

Figure 3. Excitation profiles of (py-h_5)$_2$Fe^{II}MP between 457.9 and 514.5 nm. The curve marked abs. is the absorption spectrum.

hancements within this absorption band. Although there is some scatter in the experimental data, the bound pyridine modes all maximize near 496 nm, and we assign the 0–0 transition to this wavelength. None of the excitation profiles shows evidence of a strong 0–1 maximum, with the possible exception of the 635- and 179-cm^{-1} modes, whose 0–1 positions are difficult to resolve. This behavior suggests that the origin shifts in the excited state are not large (vide infra).

Excited-State Geometry. For totally symmetric modes, the extent of resonance enhancement depends mainly on the dipole strength of the electronic transitions and on the Franck–Condon overlaps of the vibrational wave functions of the ground and excited states. It has recently been emphasized[15-17] that the relative enhancements of the Raman bands of a complex molecule contain information about the excited-state geometry. If the potential surfaces for ground and excited states can be calculated,[16] then the relative Raman intensities can be determined directly. The excited-state geometry can then be obtained from that potential surface which reproduces the observed Raman intensities. A less rigorous approach is to assume that the electronic and vibrational functions are separable and that the excited-state distortions are small so that the Franck–Condon overlaps are simply proportional to the origin shifts. Warshell[16] and also Blazej and Peticolas[17] have given the following approximate equation relating the relative intensity, I_s, to the origin shift, Δ_s, for a mode of frequency ν_s:

$$I_s \propto \nu_s^2\Delta_s^2[((\Delta\nu)^2 + \nu_s\Delta\nu - \Gamma^2)^2 + (2\Gamma\Delta\nu + \Gamma\nu_s)^2]^{-1} \quad (1)$$

Here $\Delta\nu$ is the detuning interval, namely, the difference between the laser frequency and the 0–0 electronic transition frequency, and Γ is the damping constant, proportional to the spectrally observed electronic half-width. This equation is valid for isolated modes (no combination levels are included) with small origin shifts, and negligible change in vibrational frequency or normal mode composition upon electronic excitation.[16] Despite these limitations, it seems a useful means for converting measured relative intensities into a qualitative picture of the excited-state geometry.

A set of relative Δ_s values for bound pyridine modes obtained via eq 1 was calculated from the relative intensities measured at 496 nm, where $\Delta\nu \simeq 0$; these are listed in Table II. A value of 770 cm^{-1}, the full width at half height of the best resolved pyridine profile (1216 cm^{-1}), was assumed for Γ. The origin shifts are relatively insensitive to variations in Γ, although the low-frequency modes show more sensitivity than the higher energy modes.

The normal mode origin shifts correspond to Cartesian displacements between the excited and ground equilibrium geometries Δr_i of the i pyridine atoms via the transformation[18,19]

$$\Delta r_i = (m_i)^{-1/2} \sum_s L_{si}\Delta_s/0.17\sqrt{\nu_s} \quad (2)$$

where L_{si} is the eigenvector element[9a] connecting atom i, of mass m_i, with the normal mode s. The Cartesian displacements were used to estimate relative changes in bond distances and angles between the excited and ground geometries.

Since the origin shifts are proportional to the square roots of the intensities in eq 1, their signs are undetermined. There are consequently 2^m calculable geometries, where m is the number of coupled normal modes. In the present case there are six nonzero intensities for the py-h_5 molecule and 64 possible solutions. Half of these differ only in the overall sign and not in the nature of the distortion coordinate. Table II gives the 32 solutions which involve contraction of the middle C–C bonds of the pyridine rings (vide infra). The first six columns of Table II give the phasing of the six modes, while the next four give the relative changes in the ring (C_1–N, C_1–C_2, and C_2–C_3) and Fe–N bond distances. Only relative displacements are calculable since absolute intensities have not been determined. These were scaled to produce agreement with the molecular orbital estimate (vide infra) for the C–N expansion of solution 1.

The py-d_5 intensities provide a means of distinguishing among solutions, since deuteration should not affect the excited-state geometry, but it does alter the normal mode composition. The py-d_5 intensities were calculated by a reversal of the above procedure; the 32 potential excited-state geometries, using normalized reduced mass Cartesian displacements, were each coupled to the py-d_5 eigenvectors by dot products; the 32 sets of origin shifts appropriate to py-d_5 modes were determined and py-d_5 mode intensities were calculated via eq 1 for each excited-state geometry. These were compared with the experimental values by normalizing to the most intense band (1557 cm^{-1}) and obtaining the intensity residuals; for

Table II. Calculated Geometries of the $d_\pi(Fe) \rightarrow \pi^*(py)$ Charge Transfer State

normal modes[a]						bond distortions[b]				residuals	
1	3	5	6	7	8	Δ_{CN}	$\Delta_{C_1C_2}$	$\Delta_{C_2C_3}$	Δ_{FeN}	$\Delta I\text{-}d_5$[c]	Δbonds[d]
1 −	+	−	+	+	−	0.012	−0.013	0.016	−0.020	0.635[e]	0.292
2 −	+	+	−	+	−	0.005	−0.036	0.000	−0.039	0.684	1.055
3 −	+	−	+	+	+	0.014	−0.011	0.017	0.011	0.688	0.308
4 −	+	+	−	+	+	0.011	−0.030	0.001	0.007	0.791	0.812
5 −	+	+	−	−	−	0.008	−0.033	0.001	−0.023	0.839	0.931
6 −	+	−	+	−	−	0.013	−0.013	0.016	−0.011	0.883	0.283
7 −	+	+	+	+	+	0.023	−0.007	0.011	0.005	0.978	0.335
8 −	+	−	+	−	+	0.000	−0.035	0.006	0.038	1.009	1.028
9 −	+	+	−	−	+	0.011	−0.029	0.000	0.017	1.053	0.737
10 −	−	+	−	−	−	0.004	−0.033	−0.005	−0.036	1.088	1.127
11 −	+	+	+	+	−	0.020	−0.009	0.012	−0.037	1.094	0.245
12 −	+	−	−	+	−	−0.005	−0.032	0.005	−0.011	1.144	1.104
13 −	+	+	+	−	−	0.021	−0.009	0.012	−0.026	1.202	0.240
14 +	−	−	−	+	−	0.023	−0.007	0.011	+0.003	1.263	0.323
15 −	−	−	+	−	−	0.013	−0.009	0.019	−0.018	1.272	0.415
16 −	+	−	−	+	+	−0.003	−0.034	0.005	−0.028	1.300	0.962
17 −	+	−	−	−	−	0.003	−0.033	0.006	−0.001	1.378	1.051
18 −	−	−	−	−	−	−0.009	−0.030	0.003	−0.005	1.476	1.194
19 −	−	+	+	−	−	−0.025	−0.004	0.012	−0.040	1.502	0.481
20 −	−	+	+	−	+	0.0119	−0.002	0.028	0.002	1.586	0.860
21 −	−	+	−	−	+	0.008	−0.028	−0.005	0.019	1.593	0.933
22 −	+	−	−	−	+	0.000	−0.035	0.006	0.038	1.622	1.028
23 −	−	+	−	+	−	0.000	−0.035	−0.007	−0.056	1.818	1.315
24 +	+	+	−	+	−	0.017	−0.007	0.018	0.023	1.907	0.363
25 +	+	+	−	−	+	0.013	−0.009	0.019	−0.033	2.020	0.448
26 +	+	+	+	−	−	−0.011	−0.029	0.001	−0.016	2.085	1.258
27 −	−	+	+	+	−	0.026	−0.003	0.013	−0.052	2.104	0.512
28 −	−	+	+	+	+	0.029	−0.001	0.012	−0.016	2.150	0.641
29 −	−	+	−	+	+	0.005	−0.030	−0.007	0.005	2.356	1.107
30 −	−	−	−	−	+	−0.006	−0.033	0.003	0.044	2.547	1.192
31 −	−	−	+	+	+	0.017	−0.007	0.018	0.014	2.669	0.388
32 −	−	−	−	+	+	0.009	−0.031	−0.001	0.030	3.296	1.274

[a] The table gives the signs of the origin shifts; the magnitudes of $\Delta_s/\nu_s^{1/2}$, determined from eq 1, are 1.0, 1.164, 0.502, 0.838, 0.236, and 0.355. Modes 2 and 4 have zero contribution. [b] Scaled by $|\Delta_{MO}|/\Sigma|\Delta\text{bond}|$. [c] $\Delta I\text{-}d_5 = \Sigma|I_{obsd} - I_{calcd}|/I_{1557}$ for (py-d_5)$_2$Fe^{II}MP. [d] $\Delta\text{bonds} = \Sigma|\Delta_{calcd} - \Delta_{MO}|/\Sigma|\Delta_{MO}|$ for the three ring bonds; Δ_{MO} = +0.0175, −0.0140, and +0.0102 Å for C_1N, C_1C_2, and C_2C_3, respectively. [e] Origin shifts, $\Delta_s/\nu_s^{1/2}$, for (py-d_5)$_2$Fe^{II}MP are 1.0, 0.359, 0.602, 0.284, 0.254, 0.766, 0.246, 0.310.

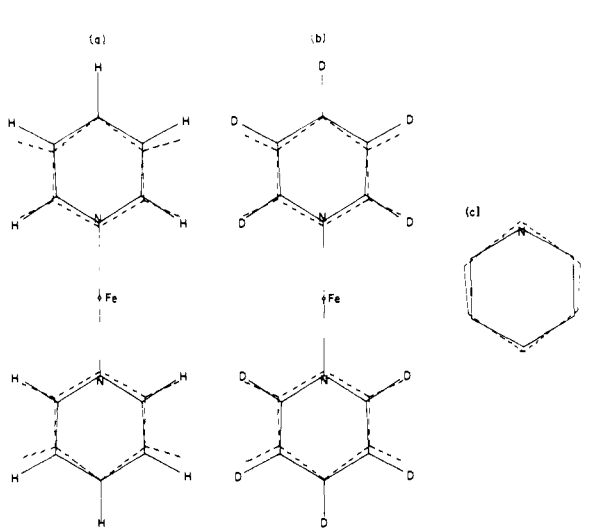

Figure 4. Excited-state distortion given by solution 1 of Table II for Fe(py-h_5)$_2$ (a) and Fe(py-d_5)$_2$ (b), compared with the calculated distortion (c), upon placing half an electron in the first π^* orbital of pyridine (see text). The solid and dashed lines represent the ground- and excited-state geometries, respectively. The bond stretching distortions are given in Table II. The angular distortions of the hydrogens are 2–4°.

py-d_5 there are eight bands with nonzero intensity, providing seven independent checks. The solutions in Table II are ranked according to increasing sums of the absolute values of the residuals, listed in column 11. The three best solutions have comparable sums 0.64, 0.68, and 0.69, corresponding to 64–69% of the intensity of the strongest band, or an average of 9–10% per band. This is outside of experimental error, perhaps reflecting an imperfect normal mode determination, but more likely resulting from the approximations in the intensity relationship of eq 1. Since the magnitudes of these effects are unknown, we cannot at this stage be certain that any of the three best solutions is correct; there is no sharp increase for the remaining sums of the residuals, only a gradual one.

It can be observed, however, that the first three solutions display the expected kind of distortion for a state in which electron density is transferred to the lowest π^* orbital of pyridine. This orbital has a pair of nodes bisecting the C_1–N and outer C–C (C_2–C_3) bonds; these are expected to expand, while the middle C–C bond (C_1–C_2) is expected to contract. This is what is found for solutions 1–3 and for several of the other solutions.

To place the comparison with expected bond-distance changes on a more quantitative basis, we have used the molecular orbital coefficient calculated by Goodman[20] for the lowest π^* orbital, obtaining the wave function

$$\psi_{\pi^*} = 0.374\phi_N - 0.519(\phi_{C_1} + \phi_{C_5}) - 0.299(\phi_{C_2} + \phi_{C_4}) + 0.378\phi_{C_3}$$

The change in bond order with respect to the ground state was then estimated as the product of the π^* coefficients of the bonded atoms, multiplied by one-half, on the assumption that the transferred electron is spread over both py rings in the charge transfer state. Finally a linear relation[21] was assumed

between the bond distance, d, and the π bond order, p:

$$d = S - (S - D)p \quad (3)$$

where S and D are standard single and double bond distances: S = 1.517 and 1.470 Å and D = 1.337 and 1.290 Å for C–C and C_1–N distances, respectively.[22] The changes in the pyridine bond distances (Δ_{MO}) were calculated to be +0.0175, −0.0140, and +0.0102 Å for C_1–N, C_1–C_2, and C_2–C_3, respectively. The last column of Table II lists the sum of the absolute values of the residuals between "observed" and calculated normalized bond length changes for the 32 solutions. Solutions 1, 3, 6, 7, 11, 13, and 14 all show sums of residuals near 0.3, significantly lower than the remaining solutions. Among this set, solutions 1 and 3 have significantly better deuterium residuals than the remainder.

Solutions 1 and 3 differ only in the sign of the origin shift of mode 8, the Fe–N stretching mode. This coordinate is not strongly mixed into the other modes, and the excited-state distortions differ mainly in the sign of the Fe–N bond length change. Figure 4 illustrates the similarity in the form of the excited-state distortion provided by solution 1 and the MO calculation. We expect a contraction of the Fe–N bond, since the Fe→ py charge-transfer transition increases the positive charge on Fe and the negative charge on py, thereby increasing the bond polarity. Consequently solution 1, which has the best deuterium residual, a satisfactory MO bond displacement residual, and the expected sign of the Fe–N displacement, is provisionally assigned as the correct solution. It corresponds to an excited-state geometry in which the C_1–C_2 bonds are contracted by about as much as the N–C_1 and C_2–C_3 bonds are expanded (0.012–0.016 Å) and the Fe–N bond is contracted by a slightly larger amount, 0.020 Å. The scaling depends on the accuracy of the MO calculation, and could be corrected by an absolute intensity measurement, or by a complete analysis of the excitation profiles.[16]

Acknowledgment. We thank Professor A. Warshel and W. L. Peticolas for helpful comments. This work was supported by NIH Grant HL 12526 and NSF Grant CHE 74-00055.

References and Notes

(1) T. G. Spiro and J. M. Burke, *J. Am. Chem. Soc.*, **98**, 5482 (1976).
(2) H. Kobayashi and Y. Yanagawa, *Bull. Chem. Soc. Jpn.*, **45**, 450 (1972).
(3) J. M. Burke, J. R. Kincaid, S. Peters, R. R. Gagne, J. P. Collman, and T. G. Spiro, *J. Am. Chem. Soc.*, **100**, 6083 (1978).
(4) T. G. Spiro and T. M. Loehr, *Adv. Infrared Raman Spectrosc.*, **1**, 98–142 (1975).
(5) H. Brunner, *Naturwissenschaften*, **61**, 129 (1974).
(6) J. Kincaid and K. Nakamoto, *Spectrosc. Lett.*, **9**, 19 (1976).
(7) T. Kitagawa, M. Abe, Y. Kyogoku, H. Ogoshi, E. Watanabe, and Z. Yoshida, *J. Phys. Chem.*, **80**, 1181 (1976).
(8) S. A. Asher, L. E. Vickery, T. M. Schuster, and K. Sauer, *Biochemistry*, **16**, 5849 (1977).
(9) (a) J. H. Schachtschneider, Technical Report No. 231-64 and 57-65, Shell Development Co., Emeryville, Calif., 1964–1965. (b) The L matrix as defined by Schactschneider is already mass weighted and eq 2 becomes $\Delta r_i = \sum_s L_{si}\Delta_s/0.17\sqrt{\nu_s}$.
(10) J. C. Duinker and I. M. Mills, *Spectrochim. Acta, Part A*, **24**, 417 (1968).
(11) B. Bak, L. Hansen and J. Rastrup-Andersen, *J. Chem. Phys.*, **22**, 2013 (1954).
(12) J. L. Hoard in "Porphyrins and Metalloporphyrins", K. M. Smith, Ed., American Elsevier, New York, 1975, pp 317–376.
(13) L. Corrsin, B. J. Fax, and R. C. Lord, *J. Chem. Phys.*, **21**, 1170 (1953).
(14) D. A. Long, F. S. Murfin, and E. L. Thomas, *Trans. Faraday Soc.*, **59**, 12 (1963).
(15) A. Y. Hirakawa and M. Tsuboi, *Science*, **188**, 359 (1975).
(16) (a) A. Warshel, *Annu. Rev. Biophys. Bioeng.*, **6**, 273 (1977); (b) A. Warshel and M. Karplus, *J. Am. Chem. Soc.*, **96**, 5677 (1974).
(17) D. C. Blazej and W. L. Peticolas, *Proc. Natl. Acad. Sci. U.S.A.*, **74**, 2639 (1977).
(18) E. F. Sharp and H. M. Rosenstock, *J. Chem. Phys.*, **41**, 3453 (1964).
(19) A. Warshel, *Isr. J. Chem.*, **11**, 709 (1973).
(20) L. Goodman, *J. Mol. Spectrosc.*, **6**, 109 (1961).
(21) I. Fischer-Hjalmars, *Pure Appl. Chem.*, **11**, 571 (1965).
(22) B. Bak, J. L. Mahler, L. Nygaard, and S. O. Sovensen, *J. Mol. Spectrosc.*, **2**, 361 (1958).

η^5-Cyclohexadienyltricarbonylchromium(0) Complexes from Addition of Carbon Nucleophiles to η^6-Benzenetricarbonylchromium(0). Formation, Chemical and Spectroscopic Features, and X-ray Diffraction Analysis

M. F. Semmelhack,* H. T. Hall, Jr., R. Farina, M. Yoshifuji, G. Clark, T. Bargar, K. Hirotsu, and J. Clardy

Contribution from the Department of Chemistry, Cornell University, Ithaca, New York 14853. *Received August 4, 1978*

Abstract: The addition of reactive carbanions to η^6-benzenetricarbonylchromium(0) produced η^5-(6-alkylcyclohexadienyl)tricarbonylchromium(0) anion complexes, as the lithium salts. Reaction with a variety of oxidizing agents (iodine, cerium(IV), oxygen) removes the hydrogen from C-6 and detaches the $Cr(CO)_3$ unit, to produce a substituted arene. Reaction with electrophiles (potential hydride acceptors) leads to cleavage of the carbon–carbon bond at C-6 with regeneration of η^6-benzenetricarbonylchromium(0). Solution spectral (^1H NMR, IR) data are consistent with an η^5-cyclohexadienyl structure. X-ray diffraction analysis on the crystalline adduct of η^6-benzenetricarbonylchromium(0) and 2-lithio-1,3-dithane defines the mode of addition (exo), the deformation (38.6°) of C-6 from the plane of carbons 1–5 in the cyclohexadienyl ligand, and the preferred conformation of the $Cr(CO)_3$ unit.

Introduction

The π complex (**1**) of the chlorobenzene with the chromium tricarbonyl unit undergoes nucleophilic substitution for chloride under mild conditions, providing an overall conversion parallel with classical nucleophilic aromatic substitution.[1] The $Cr(CO)_3$ group enhances the reactivity of the arene ligand to a degree similar to the nitro substituent in *p*-chloronitrobenzene.[1] The preparative aspects of this reaction have been explored recently, focusing on carbon nucleophiles of special interest in organic synthesis.[2] The mechanism has been discussed[3] in terms of cyclohexadienyl anionic intermediates such

0002-7863/79/1501-3535$01.00/0